

Bonding and Reactivity of a Pair of Neutral and Cationic Heterobimetallic RuZn₂ Complexes

Fedor M. Miloserdov,* Anne-Frédérique Pécharman, Lia Sotorrios, Nasir A. Rajabi, John P. Lowe, Stuart A. Macgregor,* Mary F. Mahon, and Michael K. Whittlesey*

Cite This: *Inorg. Chem.* 2021, 60, 16256–16265

Read Online

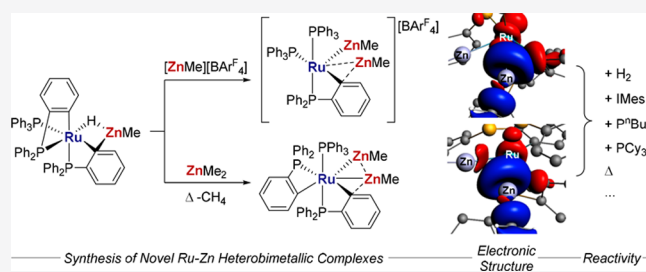
ACCESS |

Metrics & More

Article Recommendations

Supporting Information

ABSTRACT: A combined experimental and computational study of the structure and reactivity of two [RuZn₂Me₂] complexes, neutral [Ru(PPh₃)(Ph₂PC₆H₄)₂(ZnMe)₂] (**2**) and cationic [Ru(PPh₃)₂(Ph₂PC₆H₄)(ZnMe)₂][BAR^F₄] ([BAR^F₄] = [B{3,5-(CF₃)₂C₆H₃}₄]) (**3**), is presented. Structural and computational analyses indicate these complexes are best formulated as containing discrete ZnMe ligands in which direct Ru–Zn bonding is complemented by weaker Zn⋯Zn interactions. The latter are stronger in **2**, and both complexes exhibit an additional Zn⋯C_{aryl} interaction with a cyclometalated phosphine ligand, this being stronger in **3**. Both **2** and **3** show diverse reactivity under thermolysis and with Lewis bases (PⁿBu₃, PCy₃, and IMes). With **3**, all three Lewis bases result in the loss of [ZnMe]⁺. In contrast, **2** undergoes PPh₃ substitution with PⁿBu₃, but with IMes, loss of ZnMe₂ occurs to form [Ru(PPh₃)(C₆H₄PPh₂)(C₆H₄PPhC₆H₄Zn(IMes))H] (**7**). The reaction of **3** with H₂ affords the cationic trihydride complex [Ru(PPh₃)₂(ZnMe)₂(H)₃][BAR^F₄] (**12**). Computational analyses indicate that both **12** and **7** feature bridging hydrides that are biased toward Ru over Zn.



INTRODUCTION

Heterobimetallic complexes comprised of a transition metal (TM) and a main group metal (MGM) are the focus of considerable interest^{1–3} because of the possibility that the disparate chemistry of the two partners could combine cooperatively to bring about the novel stoichiometric and/or catalytic activation of small molecules.^{4–9} In one recent example, shown in Scheme 1a, the challenging C–O activation of an anisole takes place across the Rh–Al bond of complex **I** to afford **II**, which upon addition of a silane, mediates catalytic C–O bond reduction.¹⁰ Complex **I** represents one class of heterobimetallic complexes in which the MGM forms part of a multidentate ligand on the TM center.¹¹ Another class of complex is represented by **III** in Scheme 1b, in which the MGM is unsupported and unconstrained. In this particular case, both Ru and Zn centers are coordinatively unsaturated, and this “dual unsaturation” allows them to act cooperatively in the stoichiometric activation of H₂ to give **IV**.¹² We have interpreted Ru–Zn bonding within complex **III** and other related Ru–Zn complexes^{13,14} in terms of a donor–acceptor interaction between a Ru(0) metal center and Z-type Zn-based acceptor ligands.

Complex **III** is formed upon elimination of an alkane,^{15–18} an approach we have used to prepare other Ru and mono-Zn-containing products, including complex **1** in Scheme 2 that features bridging hydride and aryl ligands.^{12–14,19–21} Accordingly, the reaction of complex **1** with ZnMe₂ resulted in further

alkane elimination and formation of neutral [RuZn₂Me₂] complex **2**.¹⁴ Alternatively, reaction with a source of [ZnMe]⁺ induced C–H reductive coupling in **1** and formation of cationic [RuZn₂Me₂] complex **3**.¹³

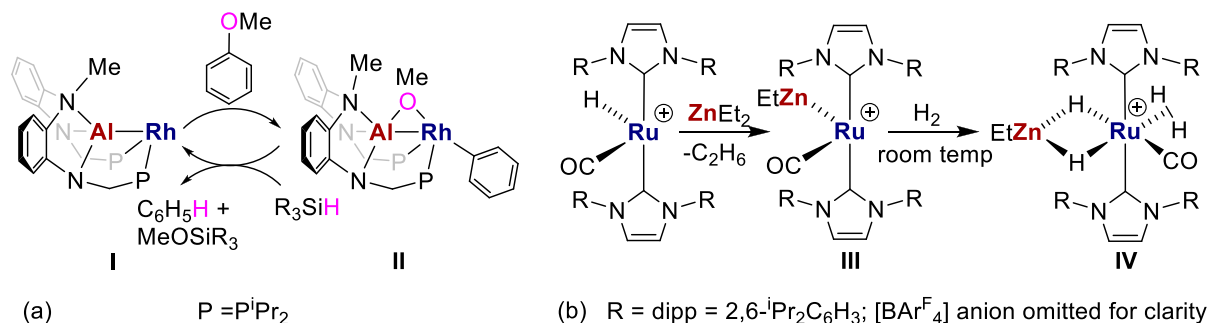
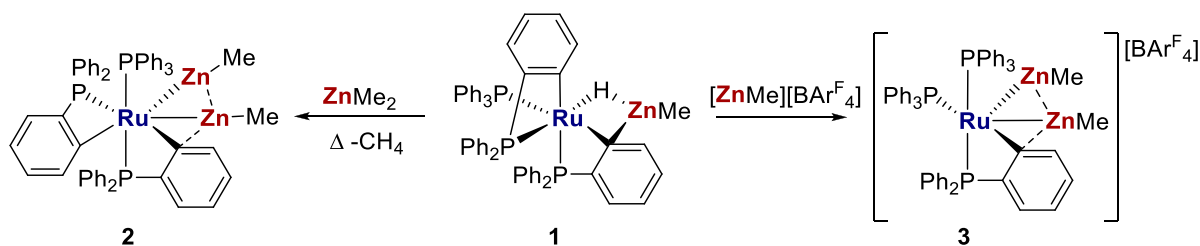
Another strategy for the preparation of [TM–Zn₂R₂] species^{23–25} involves addition of Carmona’s Cp*Zn–ZnCp* dimer to low-valent precursors.^{26,27} On the basis of the isolobal nature of Cp*Zn and a hydrogen atom, the coordination of the TM center to an intact Zn–Zn bond can be considered to form an all-metal analogue of a TM(η²-H₂) complex. Likewise, weakening of the Zn–Zn interaction to the point where it gives two ZnCp* ligands has been compared to the oxidative cleavage of the η²-H₂ ligand to form two M–H bonds, although such Zn–Zn bond cleavage is proposed to proceed without any change in the formal oxidation state.^{23,26} In such cases, ZnCp* and related ZnR (R = alkyl or aryl) ligands have been formulated as monovalent one-electron donors.²⁶ Computational studies have suggested that the extent to which the Zn–Zn interaction in Cp*Zn–ZnCp* is retained upon approach to a TM is dependent on the nature of the

Received: July 8, 2021

Published: October 18, 2021



Scheme 1. Examples of Cooperativity in Small Molecule Activation by TM–MGM Heterobimetallic Complexes

Scheme 2. Syntheses of Neutral and Cationic $[RuZn_2Me_2]$ Complexes **2** and **3**^a

^a $[BAR^F_4] = [B(3,5\text{-}(CF_3)_2C_6H_3)_4]$. The nature of the bonding between centers connected by dashed lines is investigated herein.²²

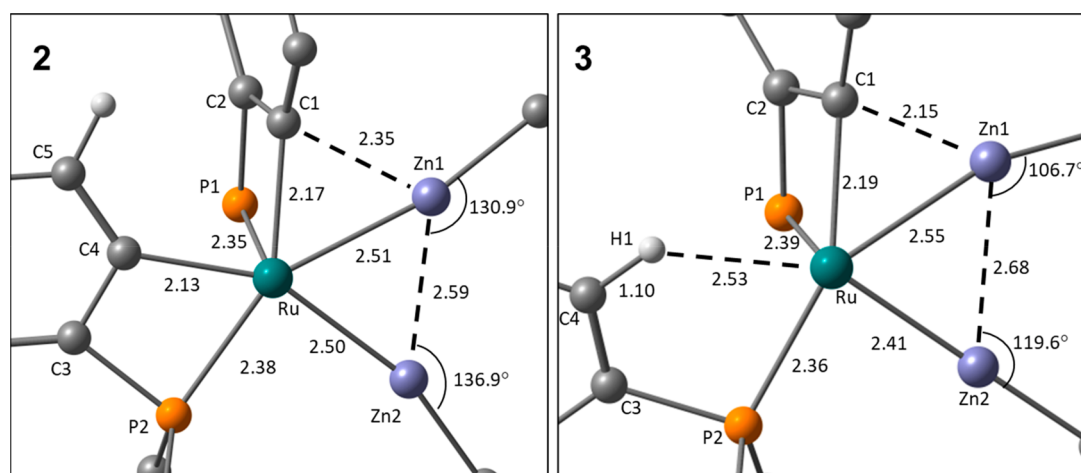


Figure 1. Geometries and labeling scheme used in the analyses of **2** and **3**, focusing on the central $RuZn_2$ core. Selected distances are given in angstroms.

metal itself, the surrounding ancillary ligands, and the ZnR substituents.^{26–28}

In this context, the availability of the closely related neutral and cationic $[RuZn_2R_2]$ complexes, **2** and **3**, respectively, provides an opportunity to explore the analogy between $\{RZn-ZnR\}$ and H_2 . Herein, we report computational and experimental studies to this end.

RESULTS AND DISCUSSION

Structure and Bonding in **2 and **3**.** Figure 1 shows the geometries and labeling system used in the discussion of **2** and **3**. In general, good agreement was seen between the experimental and fully optimized structures; however, the $Zn1\cdots C1$ distances were overestimated by 0.06–0.20 Å depending on the functional used (Supporting Information). Therefore, to analyze the observed geometries, we have taken

the heavy atom (i.e., non-H) positions from the crystallographic studies and optimized the H atom positions with the BP86 functional. This approach also allows for a consistent treatment of the new hydride-containing structures that we describe below, where the H atom location is intrinsically less precise.

Both **2** and **3** feature triangular $RuZn_2$ moieties with $Ru-Zn$ distances that are shorter than $Zn-Zn$ distances. The $Ru-Zn$ distances are more symmetrical in **2** (2.50/2.51 Å) than in **3** (2.41/2.55 Å) and are all within the sum of the covalent radii (Ru , 1.46 Å; Zn , 1.22 Å),²⁹ suggesting direct $Ru-Zn$ bonds in all cases. $Zn-Zn$ bonding in related systems has been discussed within the limits of the $Zn-Zn$ distance in $Zn_2Cp^*_2$ (2.31 Å), and the metallic radius of Zn (1.339 Å) and the $Zn-Zn$ distances in **2** and **3** (2.59 and 2.68 Å, respectively) are at the upper end of this range.²⁶ A $[TMZn_2R_2]$ unit with an intact $\eta^2-RZn-ZnR$ moiety would

also be characterized by near-linear Zn–Zn–R angles and M–Zn–R angles approaching 150° (the limit for an equilateral triangle).²⁶ In **2**, the average Zn–Zn–R and Ru–Zn–Me angles are 133.9° and 165.8°, respectively, while in **3**, the average Zn–Zn–R angle is 113.2° and the Ru–Zn2–Me angle is 179.4°. These data indicate that **2** and **3** are best formulated as Ru(ZnMe)₂ complexes, but that **2** is slightly displaced along the continuum toward a Ru(η^2 -RZn–ZnR) species.²⁶ Note that in **3**, the Ru–Zn1–Me angle is smaller than expected at 161.3°, but in this case, the Me group is bent away from C1, suggesting that it is the short Zn1...C1 contact of 2.15 Å that drives this distortion. This is explored further in the electronic structure analyses below.

Figure 2a provides details of quantum theory of atoms in molecules (QTAIM) analyses of **2** and **3** with electron density

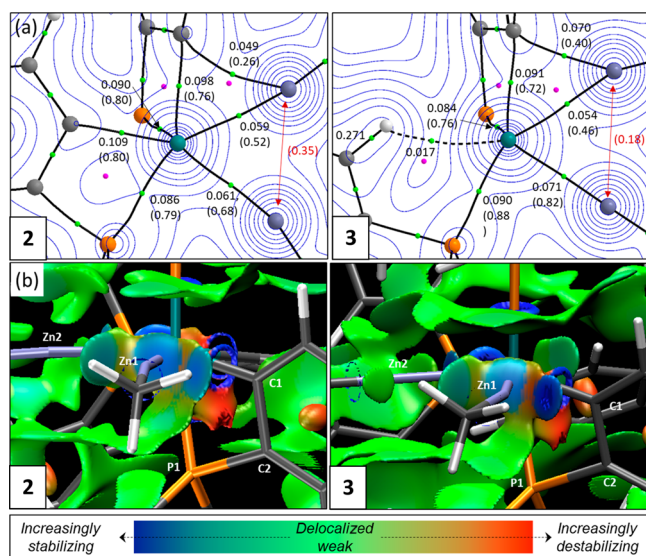


Figure 2. Electronic structure analysis of (left) **2** and (right) **3** focusing on key interactions around the {RuZn1Zn2} plane. (a) QTAIM molecular graphs with bond critical points (BCPs) in green and ring critical points (RCPs) in pink. Electron density, $\rho(r)$, contour plots are shown in the {RuZn1Zn2} plane along with selected BCP (au) and delocalization indices in parentheses; delocalization indices between atoms not linked by a bond path are colored red. (b) Detail of the NCI plots viewed from above the {RuZn1Zn2} plane and looking down the Ru–Zn1 vector. Isosurfaces are generated for $\sigma = 0.3$ au and $-0.07 < \rho < 0.07$ au; a key showing the color scheme employed is also provided.

contours plotted in the {RuZn1Zn2} plane. These are complemented by noncovalent interaction (NCI) plots shown in Figure 2b. For **2**, bond paths between Ru and both Zn centers are consistent with the presence of Ru–Zn bonds. The associated bond critical points (BCPs) show similar electron densities, $\rho(r)$, of ~ 0.06 au, and this relatively low value, coupled with positive values of the Laplacian and small negative total energy densities (Figures S39 and S40), is consistent with a donor–acceptor (i.e., Ru \rightarrow Zn) interaction between two heavy atoms.^{30,31} Figure 2a also shows the computed delocalization indices (DI) in parentheses. These reflect the degree of shared electron density between two atomic centers^{32,33} and proved more discriminating than $\rho(r)$ for the Ru–Zn interactions. Thus, a larger DI of 0.68 is associated with the shorter Ru–Zn2 bond compared to a DI of 0.52 for the Ru–Zn1 bond. DIs can also be measured between

atoms not linked by a bond path and can be useful for identifying interactions in areas of flat electron density.³⁴ A Zn1...Zn2 DI of 0.35 suggests a weak Zn...Zn interaction is present. For Zn1, this is supplemented by interaction with C1 to which a curved bond path [2.35 Å; $\rho(r) = 0.049$; DI = 0.26] indicates a degree of bridging character for the cyclometalated aryl group, albeit biased toward Ru [2.17 Å; $\rho(r) = 0.098$ au; DI = 0.76]. These stabilizing interactions are confirmed by the NCI plot of **2** that displays turquoise and blue regions along the Zn1...Zn2 and Zn1...C1 vectors, respectively.

For **3**, variations in these different interactions are seen relative to **2** that reflect changes in the interatomic distances. Thus, the Ru–Zn2 interaction strengthens [2.41 Å; $\rho(r) = 0.071$; DI = 0.82] while Ru–Zn1 interaction weakens [2.55 Å, $\rho(r) = 0.054$; DI = 0.46]. The Zn1...Zn2 interaction also weakens significantly (2.68 Å; DI = 0.18); for Zn2, this is compensated by the stronger interaction with Ru, whereas for Zn1, the interaction with C1 strengthens [2.15 Å; $\rho(r) = 0.070$; DI = 0.40]. The stronger Zn1...C1 interaction is also apparent in the NCI plot where a sharper blue disk along the Zn1...C1 vector is seen, and this is also consistent with the bending of the Ru–Zn1–Me angle away from C1 as noted above. A similar Zn...C_{aryl} interaction has been noted before in a related Ru–Zn bimetallic complex [Zn...C, 2.282(2) Å¹³], while the longer Zn–C_{aryl} distances in the asymmetrically bridged [ZnPh]₂ dimer average 2.40 Å.³⁵

A natural orbitals for chemical valence (NOCV) analysis confirmed the differences in the additional stabilizing interactions at the {Zn1Me}⁺ fragments in **2** and **3** (Figure 3). In each case, the key deformation density channel is

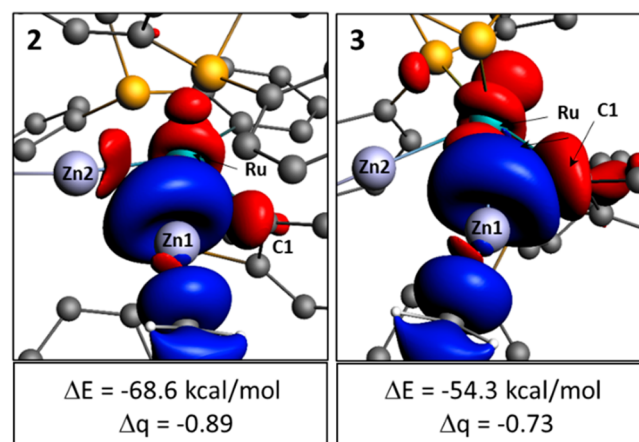
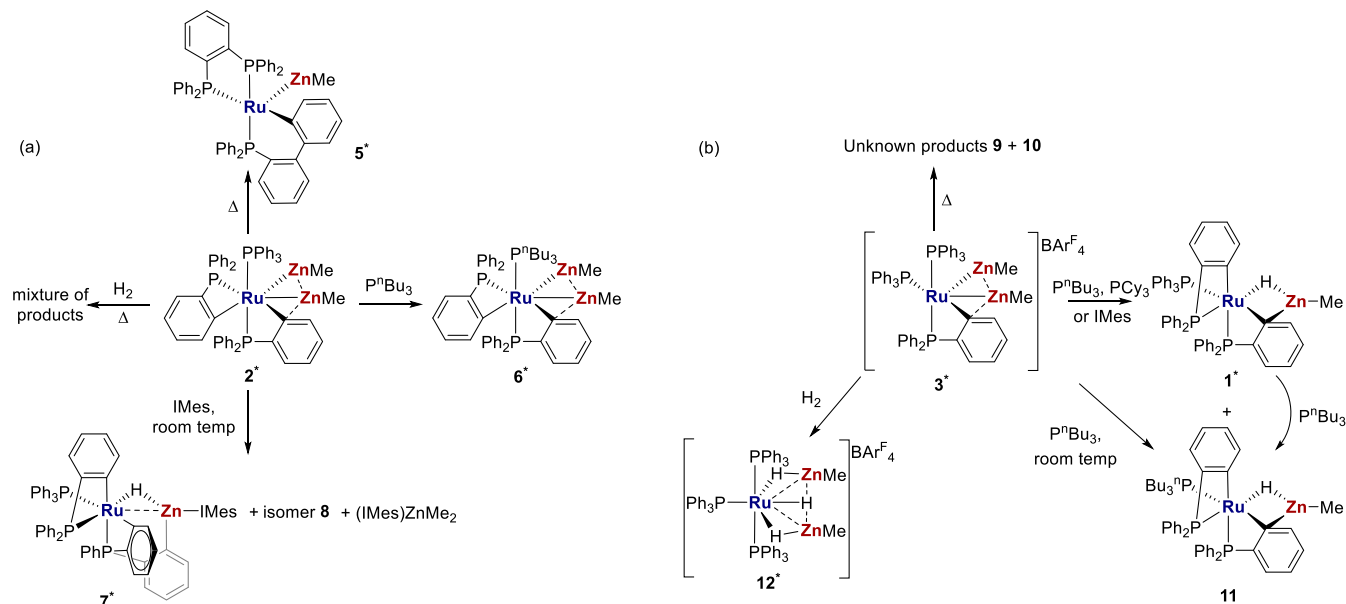


Figure 3. NOCV contour plots (isovalue of 0.0025 au) of the major deformation density channels in the interaction of the {Zn1Me}⁺ fragment with [Ru(PPh₃)(PPh₂C₆H₄)₂(ZnMe)][−] in **2** and with [Ru(PPh₃)₂(PPh₂C₆H₄)(ZnMe)] in **3**. Electron flow is shown from red to blue, and H atoms have been omitted for the sake of clarity.

dominated by donation from the *dsp* hybrid HOMO of the Ru-based fragment into the σ^* LUMO of {ZnMe}⁺. For **2**, this also shows contributions from both Zn2 and C1, whereas for **3**, a larger component from C1 is apparent but no contribution from Zn2 is seen. Equivalent plots for the {Zn2Me}⁺ fragments are provided in Figures S46 and S47.

Reactivity Studies. Given that **2** and **3** result from the formal introduction of ZnMe and [ZnMe]⁺, respectively, into **1**, a series of reactivity studies were undertaken to probe the potential to reverse this process, through either thermolysis or

Scheme 3. Reactions of (a) $[\text{Ru}(\text{PPh}_3)(\text{C}_6\text{H}_4\text{PPh}_2)_2(\text{ZnMe})_2]$ **2** and (b) $[\text{Ru}(\text{PPh}_3)_2(\text{C}_6\text{H}_4\text{PPh}_2)(\text{ZnMe})_2][\text{BAR}^{\text{F}}_4]$ **3^a**

^aStructurally characterized complexes (reported here or previously in refs 13, 14, and 20) are marked with asterisks.

reactions with Lewis bases. Such processes probe further the isolobality of ZnR and H, for example, the deprotonation of TM-hydrides. The reactions of **2** and **3** with H_2 were also attempted, and the results are summarized in panels a and b of Scheme 3.

Thermal Stabilities of 2 and 3. Heating **2** in toluene (80 °C, 2 days) resulted in the loss of ZnMe to give the previously reported $[\text{RuZnMe}]$ complex, $[\text{Ru}(\text{dppbz})(\text{PPh}_2(\text{biphenyl}))(\text{ZnMe})]$ [**5**; dppbz = 1,2-bis(diphenylphosphino)benzene; $\text{PPh}_2(\text{biphenyl})'$ = cyclometalated $\text{PPh}_2(\text{biphenyl})$], as the major product.²⁰ Alongside formal elimination of ZnMe,³⁶ the formation of **5** also requires C–H/P–C activation and C–C coupling steps to generate the dppbz and metalated $\text{Ph}_2\text{P}(\text{biphenyl})$ ligand, although the exact sequence in which these steps take place remains unknown.³⁷ For **3**, the result of heating proved to be much less clear. ³¹P NMR monitoring of a reaction mixture refluxed in benzene (2 days) or refluxed in toluene (2 h) revealed formation of an initial product **9** (characterized by two coupled doublet resonances at δ 78 and 48) that, upon further heating (2 days) in toluene, converted to a second product, **10**, which showed a similar pair of coupled signals at δ 53 and 46. Both compounds gave oils in all tested combinations of solvents,³⁸ which, together with an absence of any diagnostic (i.e., non-aromatic) ¹H NMR signals, makes their identities hard to determine.

Reactivity of 2 and 3 with Lewis Bases. Rather than removing either of the ZnMe ligands, the reaction of **2** with P^nBu_3 at room temperature led to substitution of the PPh_3 ligand and formation of $[\text{Ru}(\text{P}^n\text{Bu}_3)(\text{C}_6\text{H}_4\text{PPh}_2)_2(\text{ZnMe})_2]$ (**6**). X-ray characterization (Figure 4) revealed a structure that was broadly similar to that of **2** in terms of metrics (Table S2). The ease of phosphine substitution in **2** contrasts with the difficulties reported by Fischer in attempting to exchange phosphine ligands in multi-Zn-containing Ni species.³⁹ At the same time, the lack of reaction between **2** and PCy_3 indicates how sensitive these systems are to the choice of Lewis base. In contrast, **3** reacted with both P^nBu_3 and PCy_3 , and in this case, this did incur the loss of $[\text{ZnMe}]^+$ to give **1**, together with **11**

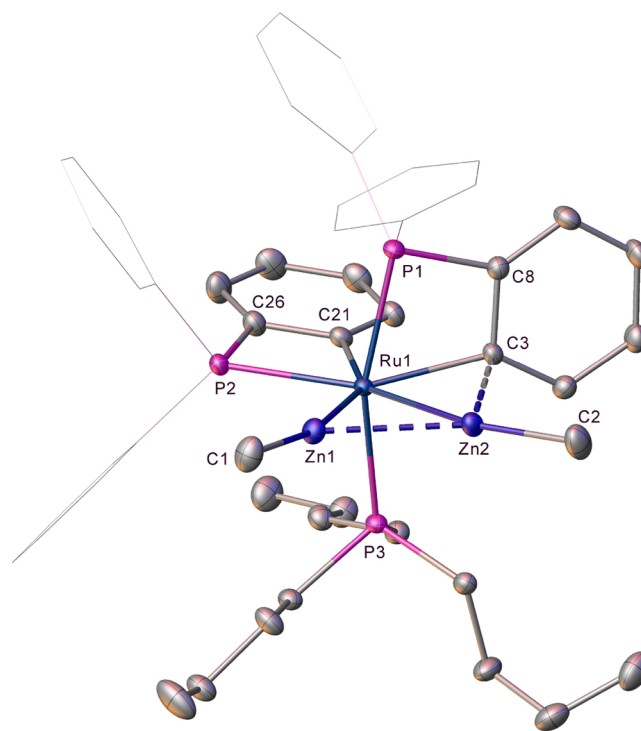


Figure 4. Molecular structure of **6**. Ellipsoids are represented at 30% probability. Hydrogen atoms and a minor disordered component have been omitted for the sake of clarity.

in the case of P^nBu_3 .^{40,41} The findings fit with the previously observed complete conversion of **3** into **1** that is seen in THF.¹³ The fate of the eliminated $[\text{ZnMe}]^+$ could not be established, but when the Lewis base is changed to the N-heterocyclic carbene IMes,⁴² trapping as the NHC adduct $[(\text{IMes})_2\text{ZnMe}]^+$ was found,⁴³ alongside formation of **1**.

A very different outcome was found when IMes was reacted with **2**. This afforded $[\text{Ru}(\text{PPh}_3)(\text{C}_6\text{H}_4\text{PPh}_2)(\text{C}_6\text{H}_4\text{PPh}_2\text{C}_6\text{H}_4\text{Zn}(\text{IMes})\text{H})]$ (**7**) through substitution of a

Me group by IMes on Zn. The formally eliminated ZnMe_2 was trapped as $(\text{IMes})\text{ZnMe}_2$ by the second equivalent of carbene necessary to bring about the full consumption of **2**.^{44,45}

The X-ray structure of **7** (Figure 5) showed a fac arrangement of an intact PPh_3 (based on P3), one phosphine

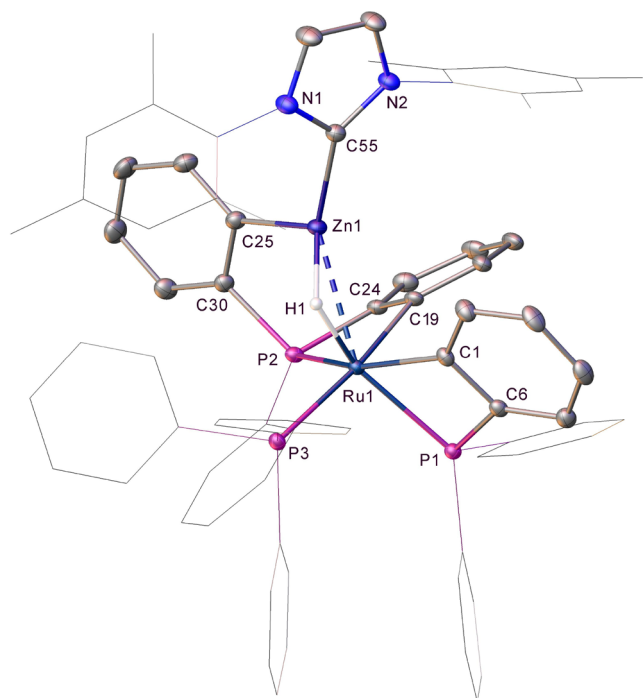


Figure 5. Molecular structure of **7**. Ellipsoids are represented at 30% probability. Hydrogen atoms (except for H1) and the solvent have been omitted for the sake of clarity.

that was cyclometalated onto ruthenium (based on P1), and a third phosphine ligand (based on P2) unusually metalated through two phenyl rings, one onto Ru [Ru1–C19, 2.1438(16) Å] and the second onto Zn [Zn1–C25, 2.0206(18) Å]. The sixth transition metal coordination site was occupied by a hydride ligand bridging the Ru and Zn centers [Ru1...Zn1, 2.6541(3) Å]. Computational analysis of the bonding in **7** is reserved until after discussion of the product of the reaction of **3** with H_2 .

Redissolving a crystalline sample of the compound gave NMR signals for **7** together with a second, minor species, **8**.⁴⁶ The signals for **7** were consistent with the solid state structure, a doublet of doublet of doublets Ru–H–Zn resonance in the ^1H NMR spectrum, with one large (pseudotrans) and two smaller $^2J_{\text{HP}}$ splittings, and one high-frequency ^{31}P triplet (δ 52) for the PPh_3 group, together with two lower-frequency (δ –12 and –24) doublet of doublet signals for the two cyclometalated phosphines.^{47,48} The presence of similar ^{31}P chemical shifts for the minor species **8** supports it being an isomer. While $^1\text{H}\{^{31}\text{P}\}$ NMR measurements showed that both isomers feature hydride *trans* to a metalated phosphine, the presence of two surprisingly small $^2J_{\text{HP}}$ couplings (9 and 6 Hz), in addition to a large, pseudotrans splitting (46 Hz) in the ^{31}P -coupled ^1H NMR spectrum, leaves it unclear as to exactly what the structure of **8** is. Closer inspection of NMR spectra recorded shortly after combining IMes and **2** indicates that **8** is formed in the initial stages (mixing for <15 min) and is thus a kinetic product of the reaction formed prior to subsequent growth of the thermodynamic product, **7**.⁴⁹ The signals of **8**

seen in the NMR spectra of **7** may therefore arise due to co-crystallization.

Reactivity of 2 and 3 toward H_2 . During our previous studies of Ru mono-Zn complexes,^{12,13,19,20} H_2 was typically found to add across the Ru–Zn bond, as shown in Scheme 1b. Very different, contrasting behavior was seen with **2** and **3**. Thus, the former did not react with H_2 at room temperature and, upon being heated to 60 °C, gave only a complex mixture of products. In contrast, **3** reacted rapidly with two molecules of H_2 at room temperature to reverse the phosphine cyclometalation and form the cationic dizinc trihydride complex, $[\text{Ru}(\text{PPh}_3)_3(\text{ZnMe})_2\text{H}_3][\text{BAR}^{\text{F}}_4]$ (**12**). Remarkably, this transformation could also be carried out in the solid state simply by stirring a powdered sample of solid **3** under 1 atm of H_2 .

Complex **12** displayed high-frequency doublet and triplet ^{31}P NMR resonances, consistent with the mer- RuP_3 geometry apparent in the X-ray crystal structure (Figure 6). The ^1H

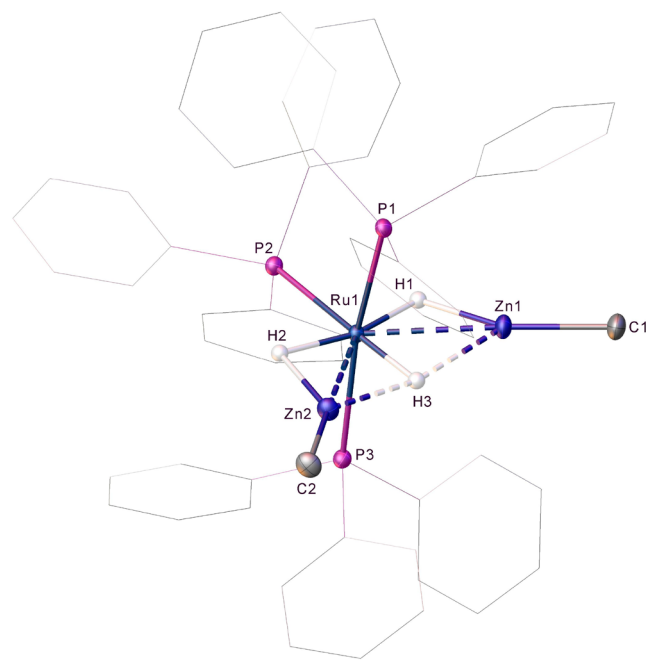


Figure 6. Molecular structure of the cation of **12**. Ellipsoids are represented at 30% probability. Phosphine and zinc methyl hydrogen atoms have been omitted for the sake of clarity.

NMR spectrum showed two hydride signals at δ –7.3 (dtd) and –11.1 (dtd) in a 2:1 ratio.⁵⁰ Upon being heated to 60 °C, **12** decomposed as evidenced by the precipitation of an insoluble red oil at the bottom of reaction solutions.

The molecular structure of the cation in **12** is shown in Figure 6. The equatorial positions comprised two ZnMe ligands, one PPh_3 ligand, and three hydrides (which were located and refined without restraints). The coordination sphere was completed by two phosphines in a distorted *trans*-axial arrangement [P1–Ru–P3, 164.804(17)°]. Two of the hydrides were disposed approximately *trans* to one another [H1–Ru–H2, 163.3(16)°], while the third was located *trans* to the equatorial PPh_3 ligand [H3–Ru–P2, 175.7(12)°]. The two Ru–Zn distances [2.5188(3) and 2.5397(3) Å] are considered further in the computational analysis of **12** below.

Structure and Bonding in 12 and 7. The computed structure of **12** and details of the QTAIM analyses are shown

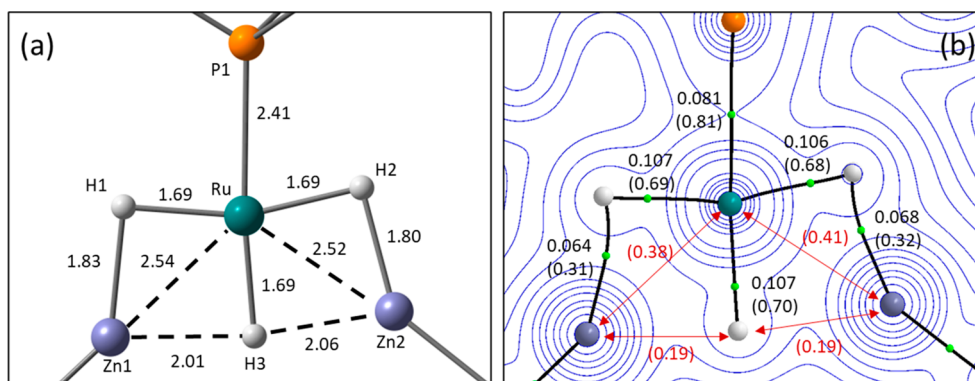


Figure 7. Electronic structure analyses of **12** highlighting key interactions in the {RuZn1Zn2} plane. (a) Computed structure of **12** (based on the experimental heavy atom positions with H atoms optimized with the BP86 functional). (b) QTAIM molecular graph with electron density contours shown in the {RuZn1Zn2} plane, with BCPs colored green with associated $\rho(r)$ (au) and delocalization indices in parentheses. Delocalization indices between selected atoms not linked by a bond path are denoted in red.

in panels a and b, respectively, of Figure 7, with the related NCI and NOCV analyses presented in the Supporting Information. In this case, QTAIM reveals an absence of Ru–Zn bond paths, despite Ru–Zn distances that are similar to those in **2** and **3**. However, the computed DIs (Ru⋯Zn1, 0.38; Ru⋯Zn2, 0.41) indicate significant Ru⋯Zn interactions are still present, and this is supported by the NCI plot that shows blue stabilizing features between Ru and both Zn centers. For the outer hydrides, H1 and H2, the computed Ru–H distances of ~ 1.69 Å are typical for a *trans* H–Ru–H arrangement and bond paths are characterized by a $\rho(r)$ of ~ 0.106 au and DIs of ~ 0.69 . These Ru–H bonds appear stronger than the Zn1–H1 and Zn2–H2 bonds [~ 1.82 Å; $\rho(r) \sim 0.065$ au; DI ~ 0.31], and these are in turn significantly weaker than the unperturbed Zn–H bond in MeZnH [1.52 Å; $\rho(r) = 0.11$ au; DI = 0.89; see Supporting Information]. H1 and H2 are therefore bridging the respective Ru–Zn vectors but are strongly biased toward Ru over Zn. This is also reflected in the very low ellipticities of the Ru–H BCPs (average of 0.028) that are indicative of terminal hydride character, compared with the higher ellipticities of the Zn–H BCPs [average of 0.48 (Figure S42)].

The properties of the Ru–H3 bond [1.69 Å; $\rho(r) = 0.107$ au, DI = 0.70] are similar to those of the Ru–H1 and Ru–H2 bonds. In this case, no bond path to either Zn center is seen but DIs of 0.19 indicate some residual interactions are still present, and these are confirmed in the NCI plot that shows turquoise regions along the Zn1⋯H3 and Zn2⋯H3 vectors. The significant ellipticity of the Ru–H3 BCP (0.145) also suggests a distortion of the electron density away from a terminal Ru–H σ -bond due to the presence of the two {ZnMe}⁺ moieties.⁵¹ An NOCV analysis of {ZnMe}⁺ bonding in **12** indicates the major deformation density channels exhibit donation from Ru and both adjacent hydrides (see the Supporting Information).

A similar analysis of the bonding in compound **7** shows the hydride present, H1, to have characteristics similar to those of H1 and H2 in **12** [Ru–H1, 1.68 Å, $\rho(r) = 0.108$, DI = 0.68; Zn–H1, 1.79 Å, $\rho(r) = 0.067$, DI = 0.33]. The Ru–Zn distance of 2.65 Å is the longest of the species studied here, and no Ru–Zn bond path is computed; however, a Ru⋯Zn DI of 0.29 suggests some interaction between the two metal centers (Figure S41).

Overall, the {Ru(H1)Zn1(H3)} and {Ru(H2)Zn2(H3)} moieties in **12** and the {RuH1Zn} moiety in **7** can be

considered as featuring asymmetrically bound bridging hydride ligands that interact more strongly with the Ru centers. A similar situation is seen in [Ru(IPr)₂(CO)(ZnR)(η^2 -H₂)-(H)₂]⁺ and [Ru(IPr)₂(CO)(ZnR)(H)₂]⁺ species (R = Et or Me),¹² where, depending on the nature of the *trans* ligand, the hydride within a {RuHZn} moiety shows different degrees of Ru–H or Zn–H bonding character. These add to the continuum of structures that can be accessed in TM–MG heterobimetallic complexes featuring hydride ligands, the precise nature of which will depend on the coordination environment of the TM partner.^{52,53}

CONCLUSIONS

A combined computational and experimental study has been undertaken on two [RuZn₂Me₂] species, neutral **2** and cationic **3**. Geometrical considerations supported by computational analyses confirm the presence of direct Ru–Zn bonds in both species and suggest these are best formulated as Ru(ZnMe)₂ complexes featuring discrete ZnMe ligands. Some additional stabilization may be achieved via Zn⋯Zn interactions, and **2** and **3** both exhibit Zn⋯C_{aryl} interactions, with these being more significant in **3**.

Experimentally, the two complexes exhibit diverse reactivities with thermolysis and the addition of a range of Lewis bases bringing about different outcomes with no apparent correlation to either the overall charges of the complexes or the different strengths of the Ru–Zn interactions present. **2** reacted with H₂ to give a mixture of products, while in contrast, reaction of H₂ with **3** led cleanly to [Ru-(PPh₃)₃(ZnMe)₂H₃][BAr^F₄] (**12**). Computational analyses of this complex suggest the presence of three hydride ligands that bridge the Ru–Zn vectors asymmetrically toward Ru.

12 adds to the range of transition metal complexes that feature multiple main group metals and multiple hydride ligands that have recently attracted a great deal of attention due to the unusual bonding interactions and unusual geometries they can possess.^{54,55} Studies of their reactivity, however, remain rare.⁵⁶ In the study presented here, we have shown that both the TM and the MGM can be centers of reactivity in these heterobimetallic complexes and the factors that govern the site of reactivity will be the subject of future reports from our groups.

EXPERIMENTAL SECTION

General Comments. All manipulations were carried out under argon using standard Schlenk, high-vacuum, and glovebox techniques using dry and degassed solvents. C_6D_6 and THF- d_8 were vacuum transferred from potassium. NMR spectra were recorded at 298 K (unless otherwise stated) on Bruker Avance 400 and 500 MHz NMR spectrometers and referenced as follows: C_6D_6 (1H , δ 7.16; ^{13}C , δ 128.0), THF- d_8 (1H , δ 1.72; ^{13}C , δ 25.3), and toluene- d_8 (1H , δ 2.09). ^{31}P spectra were referenced externally to 85% H_3PO_4 (δ 0.0). Elemental analyses were performed by Elemental Microanalysis Ltd. (Okehampton, Devon, U.K.). Compounds **1**,¹³ **2**,¹⁴ **3**,¹³ and IMes⁵⁷ were prepared according to literature methods.

[Ru(P^nBu_3)($C_6H_4PPh_2$)₂(ZnMe)₂] (6**).** C_6D_6 (0.5 mL) was added to a mixture of **2** (40 mg, 0.038 mmol) and P^nBu_3 (9.5 μ L, 0.038 mM) in a J. Young's resealable NMR tube. After 15 h at room temperature, the volatiles were removed and the resulting solid was recrystallized from benzene/hexane. The microcrystalline solid was washed with hexane and dried under vacuum to give **6** as a yellow solid (18 mg, 48%). 1H NMR (500 MHz, C_6D_6): δ 8.21–8.16 (m, 2H, Ar), 7.97–7.92 (m, 2H, Ar), 7.91–7.86 (m, 2H, Ar), 7.76 (m, 1H, Ar), 7.26 (t, J = 7.6 Hz, J = 1.5 Hz, 1H, Ar), 7.18 (dt, J = 7.6 Hz, J = 1.5 Hz, 2H, Ar), 7.11–7.04 (m, 2H, Ar), 7.03–6.85 (br, 8H, Ar), 6.84–6.72 (m, 4H, Ar), 6.54–6.49 (m, 2H, Ar), 6.40–6.35 (m, 2H, Ar), 1.71–1.52 (br m, 6H, PCH_2), 1.35–1.02 (br m, 12 H, $PCH_2CH_2CH_2$), 0.84 (t, $^3J_{HH}$ = 7.5 Hz, 9H, $PCH_2CH_2CH_2CH_3$), 0.47 (s, 3H, ZnMe), –0.64 (s, 3H, ZnMe). $^{31}P\{^1H\}$ NMR (202 MHz, C_6D_6): δ 21.3 (dd, $^2J_{PP}$ = 246 Hz, $^2J_{PP}$ = 17 Hz), –23.2 (dd, J_{PP} = 25 Hz, J_{PP} = 17 Hz), –26.3 (dd, $^2J_{PP}$ = 246 Hz, $^2J_{PP}$ = 25 Hz). $^{13}C\{^1H\}$ NMR (126 MHz, C_6D_6): δ 173.9 (dt, J_{CP} = 13 Hz, J_{CP} = 10 Hz, $C_{quaternary}$), 158.4 (dd, J_{CP} = 47 Hz, J_{CP} = 4 Hz, $C_{quaternary}$), 158.2 (dd, J_{CP} = 48 Hz, J_{CP} = 9 Hz, $C_{quaternary}$), 152.8 (dd, J_{CP} = 47 Hz, J_{CP} = 2 Hz, $C_{quaternary}$), 140.7 (dt, J_{CP} = 20 Hz, J_{CP} = 3 Hz, aryl CH), 140.5–140.0 (m, $C_{quaternary}$), 138.1 (d, J_{CP} = 21 Hz, aryl CH), 133.6 (br d, J_{CP} = 12 Hz, aryl CH), 132.7 (d, J_{CP} = 9 Hz, aryl CH), 132.3 (d, J_{CP} = 11 Hz, aryl CH), 131.9 (d, J_{CP} = 10 Hz, CH), 130.8 (br d, J = 4 Hz, aryl CH), 130.6 (app t, J_{CP} = 3 Hz, aryl CH), 130.0 (br s, aryl CH), 128.8 (br d, J_{CP} = 16 Hz, aryl CH), 128.6 (d, J_{CP} = 9 Hz, aryl CH), 128.3 (d, J_{CP} = 9 Hz, aryl CH), 127.3 (d, J_{CP} = 9 Hz, aryl CH), 127.1 (br s), 127.0 (br s), 124.2 (d, J_{CP} = 7 Hz, aryl CH), 122.0 (d, J_{CP} = 8 Hz, aryl CH), 31.1 (br m, J_{CP} = 22 Hz, CH_2), 26.8 (d, J_{CP} = 3 Hz, CH_2), 24.8 (d, J_{CP} = 11 Hz, CH_2), 14.0 (s, CH_3), 11.5 (br m, $ZnCH_3$), –3.6 (s, $ZnCH_3$). Anal. Found (%): C, 60.51; H, 6.22. Calcd for $C_{50}H_{61}P_3RuZn_2$: C, 60.86; H, 6.23.

[Ru(PPh_3)($C_6H_4PPh_2$)($PPh(C_6H_4)_2Zn(IMes)H$)] (7**).** A mixture of **2** (40 mg, 0.037 mmol) and IMes (23 mg, 0.074 mmol) was added to a J. Young's resealable NMR tube. Addition of C_6D_6 (0.5 mL) led to an instantaneous change in color from red to orange-yellow. NMR spectroscopy revealed that consumption of the starting material took place over 3 h to give **7** as the main product. Removal of the volatiles under reduced pressure and recrystallization of the residue from benzene/hexane gave yellow crystals of **7**, which were washed with hexane and dried under vacuum (33 mg, 70% yield). 1H NMR (500 MHz, THF- d_8): δ 7.41 (s, 2H, Ar), 7.38 (br d, J = 6.8 Hz, 1H, Ar), 7.27 (t, J = 7.1 Hz, 1H, Ar), 7.22–7.14 (m, 4H, Ar), 7.11–7.07 (m, 1H, Ar), 7.02 (t, J = 8.0 Hz, 2H, Ar), 6.95–6.62 (m, 22H, Ar), 6.60–6.39 (m, 11H, Ar + $NCH=CHN$), 6.12 (t, J = 8.0 Hz, 1H, Ar), 5.87 (t, J = 7.5 Hz, 1H, Ar), 5.64 (m, 1H, Ar), 5.42 (t, J = 7.5 Hz, 1H, Ar), 2.16 (s, 6H, $C_6Me_3H_3$), 2.11 (s, 6H, $C_6Me_3H_3$), 1.92 (s, 6H, $C_6Me_3H_3$), –10.50 (ddd, $^2J_{HP}$ = 53.5 Hz, $^2J_{HP}$ = 23.0 Hz, $^2J_{HP}$ = 3.5 Hz, 1H, RuH). $^{31}P\{^1H\}$ NMR (162 MHz, C_6D_6): δ 52.4 (t, $^2J_{PP}$ = 25 Hz), –11.6 (dd, $^2J_{PP}$ = 27 Hz, $^2J_{PP}$ = 15 Hz), –24.0 (dd, $^2J_{PP}$ = 25 Hz, $^2J_{PP}$ = 15 Hz). Selected $^{13}C\{^1H\}$ NMR (126 MHz, C_6D_6): δ 182.9 (br d, J_{CP} = 3 Hz, C_{NHC}), 176.9 (br dm, J_{CP} = 65 Hz, C_{ipso}), 168.8 (dt, J_{CP} = 40 Hz, J_{CP} = 4 Hz, C_{ipso}), 166.5 (d, $^1J_{CP}$ = 59 Hz, C_{ipso}), 160.6 (dd, $^1J_{CP}$ = 56 Hz, $^3J_{CP}$ = 12 Hz, C_{ipso}), 154.4 (dd, J_{CP} = 48 Hz, J_{CP} = 4 Hz, C_{ipso}), 148.3 (d, $^1J_{CP}$ = 36 Hz, C_{ipso}), 21.0 (s, $C_6Me_3H_3$), 19.0 (s, $C_6Me_3H_3$), 18.5 (s, $C_6Me_3H_3$). Selected NMR data for **8**. 1H NMR (500 MHz, C_6D_6): δ –9.03 (ddd, $^2J_{HP}$ = 45.9 Hz, $^2J_{HP}$ = 8.8 Hz, $^2J_{HP}$ = 6.1 Hz, 1H, RuH). $^{31}P\{^1H\}$ NMR (162 MHz, C_6D_6): δ 57.4 (t, $^2J_{PP}$

= 18 Hz), –26.9 (t, $^2J_{PP}$ = 20 Hz), –30.9 (app t, $^2J_{PP}$ = 18 Hz). Anal. Found (%): C, 72.97; H, 5.46; N, 1.99. Calcd for $C_{75}H_{67}N_2P_3RuZn$: $0.4C_6H_6 \cdot 0.1C_6H_{14}$: C, 72.31; H, 5.51; N, 2.16 [NMR spectroscopy confirmed the presence of benzene and hexane (Figure S31)].

Thermal Decomposition of 2. A $C_6D_5CD_3$ solution (0.5 mL) of **2** (10 mg, 0.01 mmol) was heated at 80 °C for 50 h, affording a dark red-brown colored solution. $^{31}P\{^1H\}$ NMR spectroscopy showed complete consumption of the starting material together with the formation of **5**²⁰ and a new species **4**. Selected NMR data for **4**. $^{31}P\{^1H\}$ NMR (162 MHz, $C_6D_5CD_3$): δ 87.0 (t, $^2J_{PP}$ = 25 Hz), 49.3 (dd, $^2J_{PP}$ = 249 Hz, $^2J_{PP}$ = 24 Hz), 44.4 (dd, $^2J_{PP}$ = 249 Hz, $^2J_{PP}$ = 26 Hz).

Thermal Decomposition of 3. A C_6D_6 solution (0.5 mL) of **3** (40 mg, 0.02 mmol) was heated at 80 °C for 2 days. $^{31}P\{^1H\}$ NMR spectroscopy showed no remaining starting material and the formation of two doublet resonances for a new product **9** at δ 77.5 (J_{PP} = 38 Hz) and δ 47.7 (J_{PP} = 38 Hz). When a second sample was prepared and heated at 110 °C for 3 days, $^{31}P\{^1H\}$ NMR spectroscopy revealed total consumption of **3** and the appearance of two doublets at δ 52.8 (J_{PP} = 31 Hz) and δ 46.5 (J_{PP} = 31 Hz), which we assign to a second product, **10**.

Reaction of 3 with Lewis Bases. (i) PBu_3 (2.6 μ L, 0.01 mmol) was added to a C_6D_6 (0.5 mL) solution of **3** (20 mg, 0.01 mmol) in a J. Young's resealable NMR tube to give a homogeneous red solution. After ~15 min, deposition of an unknown, insoluble red oil started to occur. A 1H NMR spectrum of the sample at this time showed the presence of a doublet of doublet of doublets hydride signal at δ –8.25 corresponding to **1** and a second doublet of doublet of doublets hydride signal at δ –9.07 ($^2J_{HP}$ = 50.9, 21.8, and 12.3 Hz), for $[Ru(P^nBu_3)(C_6H_4PPh_2)_2(ZnMe)H]$ (**11**). (ii) PCy_3 (3 mg, 0.02 mmol) and **3** (20 mg, 0.01 mmol) were dissolved in C_6D_6 (0.5 mL) in a J. Young's resealable NMR tube to give a homogeneous red solution. After ~15 min, deposition of an unknown, insoluble red oil started to occur. A 1H NMR spectrum of the sample at this time showed the presence of a doublet of doublet of doublets hydride signal at δ –8.25 corresponding to **1**. (iii) IMes (3 mg, 0.01 mmol) and **3** (20 mg, 0.01 mmol) were dissolved in C_6D_6 (0.5 mL) in a J. Young's resealable NMR tube to give a homogeneous red solution. After ~30 min, deposition of an unknown, insoluble red oil started to occur. A 1H NMR spectrum of the solution displayed resonances for **3** alongside the diagnostic hydride of **1**. Addition of a second equivalent of IMes (3 mg, 0.01 mmol) afforded full conversion of **3** to **1**. Isolation of a small number of crystals confirmed the same unit cell parameters reported for **1**.

[Ru(PPh_3)₃(ZnMe)₂H₃][BAR^F_4] (12**).** A J. Young's resealable ampule was charged with a C_6H_6 (5 mL) suspension of **3** (96 mg, 0.05 mmol). After being gently heated to fully dissolve the solid, the resulting red solution was degassed (three freeze–pump–thaw cycles) and H_2 (1 atm) added with vigorous stirring. After 5 min, this gave a pale-yellow solution, which upon treatment with hexane (5 mL) afforded a pale-yellow crystalline sample of **12**. This was collected and dried under vacuum. Yield: 76 mg (79%). An alternative route to **12** involved stirring a solid sample of **3** under H_2 (1 atm) for ~2 h, by which time the sample had changed color from red-orange to off-white. A ^{31}P NMR spectrum in C_6D_6 revealed complete conversion to **12**. 1H NMR (500 MHz, C_6D_6): δ 8.47 (s, 8H, BAR^F_4), 7.71 (s, 4H, BAR^F_4), 7.07 (br t, 1H, J = 9.1 Hz, 6H, Ar), 7.04–6.99 (m, 12H, Ar), 6.85 (t, J = 7.3 Hz, 9H, Ar), 6.78 (t, J = 7.4 Hz, 12H, Ar), 6.71 (td, J = 7.8 Hz, J = 1.4 Hz, 6H, Ar), –1.02 (s, 6H, ZnMe), –7.34 (dtd, $^2J_{HP}$ = 16.1 Hz, $^2J_{HP}$ = 12.5 Hz, $^2J_{HH}$ = 3.3 Hz, 2H, RuH), –11.06 (dtd, $^2J_{HP}$ = 39.5 Hz, $^2J_{HP}$ = 18.1 Hz, $^2J_{HH}$ = 3.3 Hz, 1H, RuH). $^{31}P\{^1H\}$ NMR (202 MHz, C_6D_6): δ 47.4 (t, $^2J_{PP}$ = 26 Hz), 41.8 (d, $^2J_{PP}$ = 26 Hz). $^{13}C\{^1H\}$ NMR (126 MHz, C_6D_6): δ 162.8 (1:1:1:1 q, $^1J_{CB}$ = 50 Hz, BAR^F_4), 135.6–135.1 (m), 133.9 (d, J_{CP} = 11 Hz, $C_{ortho-PPh_3}$), 133.7–133.2 (m, 133.6, $C_{ipso-PPh_3}$ overlapped with 133.4, vt, J_{CP} = 6 Hz, $C_{ortho-PPh_3}$), 131.3 (s, $C_{para-PPh_3}$), 130.4–129.5 (m, 130.3, s, $C_{para-PPh_3}$ overlapped with 130.0, qq, J_{CF} = 32 Hz, J_{CF} = 3 Hz, BAR^F_4), 129.2 (vt, J_{CP} = 5 Hz, $C_{meta-PPh_3}$), 128.3 (d, J_{CP} ~ 5 Hz, $C_{meta-PPh_3}$ overlapped with C_6D_6), 125.3 (q, $^1J_{CF}$ = 273 Hz, BAR^F_4), 118.1 (s,

BAr₄^F). –5.7 (s, ZnMe). Anal. Found (%): C, 55.19; H, 3.48. Calcd for C₈₈H₆₆BF₂₄Zn₂P₃Ru: C, 55.19; H, 3.47.

X-ray Crystallography. Data for **6**, **7**, and **12** were obtained using an Agilent SuperNova instrument and a Cu K α radiation source. All experiments were conducted at 150 K, and models refined using SHELXL⁵⁸ via the Olex2⁵⁹ interface. Refinements were largely straightforward, and only points of note will be detailed herein. First, the phenyl rings based on C9 and C15 were treated for 80:20 disorder in the structure of **6**. In **7**, the asymmetric unit was seen to contain one molecule of the bimetallic complex and two molecules of benzene. The hydride in the former was located and refined without restraints as were the hydride ligands in **12**. Unsurprisingly, the anion in the latter structure required some disorder modeling. In particular, fluorine atoms F4–F6 were treated for three-way disorder in a 0.425:0.425:0.15 ratio, while F22–F24 were modeled to take into account 50:50 disorder. Distances and ADP restraints were employed in disordered regions, to assist convergence.

Computational Details. Density functional theory calculations were performed with Gaussian 16 (revision C.01).⁶⁰ Ru, Zn, and P centers were described with the Stuttgart RECPs and associated basis sets,⁶¹ and 6-31G** basis sets were used for all other atoms.^{62,63} A set of d orbital polarization functions was also added to P ($\zeta^d = 0.387$).⁶⁴ Electronic structure analyses were performed on geometries using the heavy atom positions derived from the crystallographic studies with H atom positions optimized with the BP86 functional.^{65,66} Details of functional testing on the fully optimized structure of **2** are provided in the Supporting Information. Quantum theory of atoms in molecules (QTAIM)⁶⁷ used the AIMALL program.⁶⁸ NCI calculations were based on the promolecular densities and used NCIPLOT⁶⁹ with visualization via VMD.⁷⁰ Natural orbitals for chemical valence (NOCV) analyses⁷¹ were performed using the Amsterdam Modeling Suite (AMS) package.⁷² Computed geometries are displayed with ChemCraft,⁷³ and all geometries are supplied as a separate XYZ file (Supporting Information).

■ ASSOCIATED CONTENT

SI Supporting Information

The Supporting Information is available free of charge at <https://pubs.acs.org/doi/10.1021/acs.inorgchem.1c02072>.

NMR spectra of products from reactions of **2** and **3**, X-ray structural data and metrics for **6**, **7**, and **12**, and computational details (functional testing, electronic structure analyses, QTAIM, and NOCV) (PDF)

Structures and Cartesian coordinates (XYZ)


Accession Codes

CCDC 2083542–2083544 contain the supplementary crystallographic data for this paper. These data can be obtained free of charge via www.ccdc.cam.ac.uk/data_request/cif, or by emailing data_request@ccdc.cam.ac.uk, or by contacting The Cambridge Crystallographic Data Centre, 12 Union Road, Cambridge CB2 1EZ, UK; fax: +44 1223 336033.

■ AUTHOR INFORMATION

Corresponding Authors

Fedor M. Miloserdov – Department of Chemistry, University of Bath, Bath BA2 7AY, U.K.; Laboratory of Organic Chemistry, Wageningen University, Wageningen 6708 WE, The Netherlands; Email: fedor.miloserdov@wur.nl

Stuart A. Macgregor – Institute of Chemical Sciences, School of Engineering and Physical Sciences, Heriot-Watt University, Edinburgh EH14 4AS, U.K.;  orcid.org/0000-0003-3454-6776; Email: s.a.macgregor@hw.ac.uk

Michael K. Whittlesey – Department of Chemistry, University of Bath, Bath BA2 7AY, U.K.;  orcid.org/0000-0002-5082-3203; Email: m.k.whittlesey@bath.ac.uk

Authors

Anne-Frédérique Pécharman – Department of Chemistry, University of Bath, Bath BA2 7AY, U.K.

Lia Sotorrios – Institute of Chemical Sciences, School of Engineering and Physical Sciences, Heriot-Watt University, Edinburgh EH14 4AS, U.K.

Nasir A. Rajabi – Institute of Chemical Sciences, School of Engineering and Physical Sciences, Heriot-Watt University, Edinburgh EH14 4AS, U.K.

John P. Lowe – Department of Chemistry, University of Bath, Bath BA2 7AY, U.K.

Mary F. Mahon – Department of Chemistry, University of Bath, Bath BA2 7AY, U.K.

Complete contact information is available at:

<https://pubs.acs.org/10.1021/acs.inorgchem.1c02072>

Notes

The authors declare no competing financial interest.

■ ACKNOWLEDGMENTS

This project has received funding from the European Union's Horizon 2020 research and innovation programme under Marie Skłodowska-Curie Grant Agreement 792674 (F.M.M.) and EPSRC (Grant EP/T019743/1 for A.-F.P., Grant EP/T019876/1 for L.S., and Grant EP/R020752/1 for N.A.R.).

■ DEDICATION

The authors dedicate this paper to Professor Christian Bruneau in recognition of his outstanding contributions to ruthenium chemistry.

■ REFERENCES

- (1) Liddle, S. T., Ed. *Molecular Metal-Metal Bonds: Compounds, Synthesis, Properties*; Wiley-VCH: Weinheim, Germany, 2015.
- (2) Bouhadir, G.; Bourissou, D. Complexes of amphiphilic ligands: reactivity and catalytic applications. *Chem. Soc. Rev.* **2016**, *45*, 1065–1079.
- (3) Campos, J. Bimetallic cooperation across the periodic table. *Nat. Rev. Chem.* **2020**, *4*, 696–702.
- (4) Cammarota, R. C.; Vollmer, M. V.; Xie, J.; Ye, J. Y.; Linehan, J. C.; Burgess, S. K.; Appel, A. M.; Gagliardi, L.; Lu, C. C. A bimetallic nickel-gallium complex catalyzes CO₂ hydrogenation via the intermediacy of an anionic d¹⁰ nickel hydride. *J. Am. Chem. Soc.* **2017**, *139*, 14244–14250.
- (5) Takaya, J.; Iwasawa, N. Synthesis, structure, and catalysis of palladium complexes bearing a group 13 metalloligand: Remarkable effect of an aluminum-metalloligand in hydrosilylation of CO₂. *J. Am. Chem. Soc.* **2017**, *139*, 6074–6077.
- (6) Yamada, R.; Iwasawa, N.; Takaya, J. Rhodium-catalyzed C-H activation enabled by an indium metalloligand. *Angew. Chem., Int. Ed.* **2019**, *58*, 17251–17254.
- (7) Morisako, S.; Watanabe, S.; Ikemoto, S.; Muratsugu, S.; Tada, M.; Yamashita, M. Synthesis of a pincer-Ir^V complex with a base-free aluminyl ligand and its application toward the dehydrogenation of alkanes. *Angew. Chem., Int. Ed.* **2019**, *58*, 15031–15035.
- (8) Fujii, I.; Semba, K.; Li, Q.-Z.; Sakaki, S.; Nakao, Y. Magnesianation of aryl fluorides catalyzed by a rhodium-aluminum complex. *J. Am. Chem. Soc.* **2020**, *142*, 11647–11652.
- (9) Hara, N.; Uemura, N.; Nakao, Y. C2-Selective silylation of pyridines by a rhodium-aluminum complex. *Chem. Commun.* **2021**, *57*, 5957–5960.
- (10) Seki, R.; Hara, N.; Saito, T.; Nakao, Y. Selective C-O bond reduction and borylation of aryl ethers catalyzed by a rhodium-aluminum heterobimetallic complex. *J. Am. Chem. Soc.* **2021**, *143*, 6388–6394.

- (11) Cammarota, R. C.; Clouston, L. J.; Lu, C. C. Leveraging molecular metal-support interaction for H₂ and N₂ activation. *Coord. Chem. Rev.* **2017**, *334*, 100–111.
- (12) Riddlestone, I. M.; Rajabi, N. A.; Lowe, J. P.; Mahon, M. F.; Macgregor, S. A.; Whittlesey, M. K. Activation of H₂ over the Ru–Zn bond in the transition metal–Lewis acid heterobimetallic species [Ru(IPr)₂(CO)ZnEt]⁺. *J. Am. Chem. Soc.* **2016**, *138*, 11081–11084.
- (13) Miloserdov, F. M.; Rajabi, N. A.; Lowe, J. P.; Mahon, M. F.; Macgregor, S. A.; Whittlesey, M. K. Zn-Promoted C–H reductive elimination and H₂ activation via a dual unsaturated Ru–Zn intermediate. *J. Am. Chem. Soc.* **2020**, *142*, 6340–6349.
- (14) Miloserdov, F. M.; Isaac, C. J.; Beck, M. L.; Burnage, A. L.; Farmer, J. C. B.; Macgregor, S. A.; Mahon, M. F.; Whittlesey, M. K. Impact of the novel Z-acceptor ligand bis{(ortho-diphenylphosphino)phenyl}zinc (ZnPhos) on the formation and reactivity of low-coordinate Ru(0) centers. *Inorg. Chem.* **2020**, *59*, 15606–15619.
- (15) Tebbe, F. N. Lewis acidic metal alkyl–transition metal complex interactions. 1. Niobium and tantalum hydrides. *J. Am. Chem. Soc.* **1973**, *95*, 5412–5414.
- (16) St Denis, J. N.; Butler, W.; Glick, M. D.; Oliver, J. P. Studies on main group metal–transition metal bonded compounds: II. The crystal and molecular structure of π-C₅H₅(CO)₃WGa(CH₃)₂ and evidence for mixed organozinc and organogallium transition metal derivatives. *J. Organomet. Chem.* **1977**, *129*, 1–16.
- (17) Skupiński, W. A.; Huffman, J. C.; Bruno, J. W.; Caulton, K. G. Dinuclear elimination from rhenium hydrides and AlMe₃–rhenium aluminium polyhydrides. *J. Am. Chem. Soc.* **1984**, *106*, 8128–8136.
- (18) Thorn, D. L.; Harlow, R. L. Transition metal–organoindium chemistry. Addition of alkyl–indium bonds to alkyliridium compounds and the structure of IrH(Et)(Et₂In)(PMe₃)₃. *J. Am. Chem. Soc.* **1989**, *111*, 2575–2580.
- (19) Espinal-Viguri, M.; Varela-Izquierdo, V.; Miloserdov, F. M.; Riddlestone, I. M.; Mahon, M. F.; Whittlesey, M. K. Heterobimetallic ruthenium–zinc complexes with bulky N-heterocyclic carbenes: Syntheses, structures and reactivity. *Dalton Trans.* **2019**, *48*, 4176–4189.
- (20) O’Leary, N.; Miloserdov, F. M.; Mahon, M. F.; Whittlesey, M. K. Transforming PPh₃ into bidentate phosphine ligands at Ru–Zn heterobimetallic complexes. *Dalton Trans.* **2019**, *48*, 14000–14009.
- (21) For Ru–Ga and Ru–In complexes prepared using the same approach, see: Riddlestone, I. M.; Rajabi, N. A.; Macgregor, S. A.; Mahon, M. F.; Whittlesey, M. K. Well-defined heterobimetallic reactivity at unsupported ruthenium–indium bonds. *Chem. - Eur. J.* **2018**, *24*, 1732–1738.
- (22) The depiction of species **3** in Scheme 2 differs from that in ref 13 and reflects the outcomes of our study that demonstrate direct Ru–Zn bonding and weak Zn⋯Zn and Zn⋯C_{aryl} interactions.
- (23) Bollermann, T.; Gemel, C.; Fischer, R. A. Organozinc ligands in transition metal chemistry. *Coord. Chem. Rev.* **2012**, *256*, 537–555.
- (24) Molon, M.; Gemel, C.; Fischer, R. A. From AlCp*– and GaCp*–ligated ruthenium hydrides to zinc-rich heterometallic complexes. *Eur. J. Inorg. Chem.* **2013**, *2013*, 3616–3622.
- (25) Chen, M.; Jiang, S. J.; Maron, L.; Xu, X. Transition metal-induced dehydrogenative coupling of zinc hydrides. *Dalton Trans.* **2019**, *48*, 1931–1935.
- (26) Freitag, K.; Molon, M.; Jerabek, P.; Dilchert, K.; Rosler, C.; Seidel, R. W.; Gemel, C.; Frenking, G.; Fischer, R. A. Zn⋯Zn interactions at nickel and palladium centers. *Chem. Sci.* **2016**, *7*, 6413–6421.
- (27) Ayala, R.; Carmona, E.; Galindo, A. The dizinc bond as a ligand: A computational study of elongated dizinc bonds. *Inorg. Chim. Acta* **2018**, *470*, 197–205.
- (28) Ayala, R.; Galindo, A. A QTAIM and DFT study of the dizinc bond in non-symmetric [CpZn₂L_n] complexes. *J. Organomet. Chem.* **2019**, *898*, 120878.
- (29) Cordero, B.; Gómez, V.; Platero-Prats, A. E.; Revés, M.; Echeverría, J.; Cremades, E.; Barragán, F.; Alvarez, S. Covalent radii revisited. *Dalton Trans.* **2008**, 2832–2838.
- (30) Lepetit, C.; Fau, P.; Fajerweg, K.; Kahn, M. L.; Silvi, B. Topological analysis of the metal–metal bond: A tutorial review. *Coord. Chem. Rev.* **2017**, *345*, 150–181.
- (31) Macchi, P.; Proserpio, D. M.; Sironi, A. Experimental electron density in a transition metal dimer: Metal–metal and metal–ligand bonds. *J. Am. Chem. Soc.* **1998**, *120*, 13429–13435.
- (32) Merino, G.; Vela, A.; Heine, T. Description of electron delocalization via the analysis of molecular fields. *Chem. Rev.* **2005**, *105*, 3812–3841.
- (33) Outeiral, C.; Vincent, M. A.; Martín Pendás, Á.; Popelier, P. L. A. Revitalizing the concept of bond order through delocalization measures in real space. *Chem. Sci.* **2018**, *9*, 5517–5529.
- (34) Farrugia, L. J.; Evans, C.; Lentz, D.; Roemer, M. The QTAIM approach to chemical bonding between transition metals and carbocyclic rings: A combined experimental and theoretical study of (η⁵-C₅H₅)Mn(CO)₃, (η⁶-C₆H₆)Cr(CO)₃, and (E)-{(η⁵-C₅H₄)CF=CF(η⁵-C₅H₄)}(η⁵-C₅H₅)₂Fe₂. *J. Am. Chem. Soc.* **2009**, *131*, 1251–1268.
- (35) Markies, P. R.; Schat, G.; Akkerman, O. S.; Bickelhaupt, F.; Smeets, W. J. J.; Spek, A. L. Coordinational behavior of solvent-free diorganylzinc compounds: The remarkable X-ray structure of dimeric diphenylzinc. *Organometallics* **1990**, *9*, 2243–2247.
- (36) The speciation of the eliminated ZnMe moiety was not established.
- (37) NMR monitoring of the reaction showed that after heating for 1 day, **2** and **5** were both present, alongside a major intermediate that was tentatively assigned as the BIPHEP [BIPHEP = 2,2′-bis(diphenylphosphino)biphenyl] complex [Ru(BIPHEP)(PPh₃)(ZnMe)₂] (**4**) based on the similarity of the ³¹P NMR data [δ 87 (t, J_{PP} = 25 Hz), **49** (dd, J_{PP} = 248 Hz, J_{PP} = 24 Hz), **44** (dd, J_{PP} = 248 Hz, J_{PP} = 26 Hz)] to those of Ru(BIPHEP)(PPh₃)HCl [δ 87 (dd, J_{PP} = 38 Hz, J_{PP} = 21 Hz), **41** (dd, J_{PP} = 305 Hz, J_{PP} = 38 Hz), **36** (dd, J_{PP} = 305 Hz, J_{PP} = 21 Hz)].²⁰ The presence of the BIPHEP ligand and two ZnMe ligands (two X-type ligands are necessary in combination with the three L-type ligands to give a neutral Ru species) implies that the C–C coupling needed for BIPHEP formation, Chaudret, B.; Cole-Hamilton, D. J.; Wilkinson, G. Bis(styrene)bis(triphenylphosphine)ruthenium(0) and its reactions with triphenylphosphine and with alkenes. *J. Chem. Soc., Dalton Trans.* **1978**, 1739–1745. precedes Ru–Zn cleavage and elimination of a ZnMe group.
- (38) These involved attempted crystallisation from C₆D₆, C₆D₆/hexane, C₆D₆/pentane, toluene (both room temperature and –35 °C), toluene/hexane, toluene/pentane, THF (room temperature and –35 °C), THF/hexane, THF/pentane, C₆H₅F (room temperature and –35 °C), and C₆H₅F/hexane (room temperature and –35 °C).
- (39) HeiB, P.; Hornung, J.; Zhou, X.; Jandl, C.; Pöthig, A.; Gemel, C.; Fischer, R. A. Combined experimental and theoretical study on hampered phosphine dissociation in heteroleptic Ni/Zn complexes. *Inorg. Chem.* **2020**, *59*, 514–522.
- (40) This was independently prepared from treatment of **1** with PⁿBu₃.
- (41) The mixture of **1** and **11** was found to be unstable in a C₆D₆ solution, and over ~24 h, the hydride signals for both species merged into the baseline (Supporting Information). In part, this may result from the deposition of an insoluble red oil, resulting in the loss of material dissolved in solution. However, the formation of new signals in the ³¹P NMR spectrum, two at high frequencies and one at a low frequency, not that dissimilar to those for **3** may also suggest there is further reaction of **1** or **11** with [(PⁿBu₃)₂ZnMe]⁺, resulting in the formation of a PⁿBu₃ analogue of **3**. However, the formation of a “red oil” prevented us from isolating any such product; attempts to drive the reaction through use of >1 equiv of PⁿBu₃ led to only increased amounts of red oil.
- (42) IMes = 1,3-bis(2,4,6-trimethylphenyl)imidazol-2-ylidene.
- (43) Specklin, D.; Fliedel, C.; Gourlaouen, C.; Bruyere, J. C.; Avilés, T.; Boudon, C.; Ruhlmann, L.; Dagonne, S. N-Heterocyclic carbene based tri-organyl-Zn-alkyl cations: Synthesis, structures, and use in CO₂ functionalization. *Chem. - Eur. J.* **2017**, *23*, 5509–5519.

(44) Schnee, G. F.; Fliedel, C.; Avilés, T.; Dagorne, S. Neutral and cationic N-heterocyclic carbene zinc adducts and the BnOH/ $Zn(C_6F_5)_2$ binary mixture - characterization and use in the ring-opening polymerization of β -butyrolactone, lactide, and trimethylene carbonate. *Eur. J. Inorg. Chem.* **2013**, 2013, 3699–3709.

(45) Rit, A.; Spaniol, T. P.; Maron, L.; Okuda, J. Mixed alkyl hydrido complexes of zinc: Synthesis, structure, and reactivity. *Organometallics* **2014**, 33, 2039–2047.

(46) The 7:8 ratio was \sim 1:0.15. Variable-temperature 1H NMR measurements showed this did not change between -70 and 70 °C.

(47) Garrou, P. E. Δ_R ring contributions to ^{31}P NMR parameters of transition-metal-phosphorus chelate complexes. *Chem. Rev.* **1981**, 81, 229–266.

(48) Mohr, F.; Privér, S. H.; Bhargava, S. K.; Bennett, M. A. Ortho-metalated transition metal complexes derived from tertiary phosphine and arsine ligands. *Coord. Chem. Rev.* **2006**, 250, 1851–1888.

(49) An additional species was also formed at this early stage of the reaction but is an intermediate that was mostly consumed within \sim 3 h; its identity remains unknown.

(50) The two hydride signals at $\delta -7.3$ and -11.1 showed similar T_1 values of 400 and 540 ms, respectively (400 MHz, 300 K).

(51) The computed structure of $[Ru(PPh_3)_3H_3]^-$ (i.e., **12** with both $[ZnMe]^+$ groups removed) shows a shortening of the Ru–H3 distance from 1.69 to 1.64 Å, consistent with the $\{ZnMe\}$ groups influencing the Ru–H3 interaction in **12**. In contrast, the Ru–H1 and –H2 distances are not affected.

(52) Ekkert, O.; White, A. J. P.; Crimmin, M. R. Trajectory of approach of a zinc-hydrogen bond to transition metals. *Angew. Chem., Int. Ed.* **2016**, 55, 16031–16034.

(53) Abdalla, J. A. B.; Caise, A.; Sindlinger, C. P.; Tirfoin, R.; Thompson, A. L.; Edwards, A. J.; Aldridge, S. Structural snapshots of concerted double E–H bond activation at a transition metal centre. *Nat. Chem.* **2017**, 9, 1256–1262.

(54) Garçon, M.; Bakewell, C.; Sackman, G. A.; White, A. J. P.; Cooper, R. I.; Edwards, A. J.; Crimmin, M. R. A hexagonal planar transition-metal complex. *Nature* **2019**, 574, 390–393.

(55) Tauchert, M. E.; Okuda, J. A hexagonal planar metal complex. *Angew. Chem., Int. Ed.* **2020**, 59, 4214–4215.

(56) Butler, M. J.; Crimmin, M. R. Magnesium, zinc, aluminium and gallium hydride complexes of the transition metals. *Chem. Commun.* **2017**, 53, 1348–1365.

(57) Bantreil, X.; Nolan, S. P. Synthesis of N-heterocyclic carbene ligands and derived ruthenium olefin metathesis catalysts. *Nat. Protoc.* **2011**, 6, 69–77.

(58) Sheldrick, G. M. Crystal structure refinement with SHELXL. *Acta Crystallogr., Sect. C: Struct. Chem.* **2015**, 71, 3–8.

(59) Dolomanov, O. V.; Bourhis, L. J.; Gildea, R. J.; Howard, J. A. K.; Puschmann, H. OLEX2: a complete structure solution, refinement and analysis program. *J. Appl. Crystallogr.* **2009**, 42, 339–341.

(60) Frisch, M. J.; Trucks, G. W.; Schlegel, H. B.; Scuseria, G. E.; Robb, M. A.; Cheeseman, J. R.; Scalmani, G.; Barone, V.; Petersson, G. A.; Nakatsuji, H.; Li, X.; Caricato, M.; Marenich, A. V.; Bloino, J.; Janesko, B. G.; Gomperts, R.; Mennucci, B.; Hratchian, H. P.; Ortiz, J. V.; Izmaylov, A. F.; Sonnenberg, J. L.; Williams-Young, D.; Ding, F.; Lipparini, F.; Egidi, F.; Goings, J.; Peng, B.; Petrone, A.; Henderson, T.; Ranasinghe, D.; Zakrzewski, V. G.; Gao, J.; Rega, N.; Zheng, G.; Liang, W.; Hada, M.; Ehara, M.; Toyota, K.; Fukuda, R.; Hasegawa, J.; Ishida, M.; Nakajima, T.; Honda, Y.; Kitao, O.; Nakai, H.; Vreven, T.; Throssell, K.; Montgomery, J. A., Jr.; Peralta, J. E.; Ogliaro, F.; Bearpark, M. J.; Heyd, J. J.; Brothers, E. N.; Kudin, K. N.; Staroverov, V. N.; Keith, T. A.; Kobayashi, R.; Normand, J.; Raghavachari, K.; Rendell, A. P.; Burant, J. C.; Iyengar, S. S.; Tomasi, J.; Cossi, M.; Millam, J. M.; Klene, M.; Adamo, C.; Cammi, R.; Ochterski, J. W.; Martin, R. L.; Morokuma, K.; Farkas, O.; Foresman, J. B.; Fox, D. J. *Gaussian16*, rev. C.01; Gaussian, Inc.: Wallingford, CT, 2016.

(61) Andrae, D.; Häußermann, U.; Dolg, M.; Stoll, H.; Preuß, H. Energy-adjusted ab initio pseudopotentials for the second and third row transition elements. *Theor. Chim. Acta.* **1990**, 77, 123–141.

(62) Hehre, W. J.; Ditchfield, R.; Pople, J. A. Self-consistent molecular orbital methods XII. Further extensions of Gaussian-type basis sets for use in molecular orbital studies of organic molecules. *J. Chem. Phys.* **1972**, 56, 2257–2261.

(63) Hariharan, P. C.; Pople, J. A. The influence of polarization functions on molecular orbital hydrogenation energies. *Theor. Chim. Acta.* **1973**, 28, 213–222.

(64) Hollwarth, A.; Bohme, M.; Dapprich, S.; Ehlers, A. W.; Gobbi, A.; Jonas, V.; Kohler, K. F.; Stegmann, R.; Veldkamp, A.; Frenking, G. A set of d-polarization functions for pseudo-potential basis sets of the main group elements Al–Bi and f-type polarization functions for Zn Cd, Hg. *Chem. Phys. Lett.* **1993**, 208, 237–240.

(65) Becke, A. D. Density-functional exchange-energy approximation with correct asymptotic-behavior. *Phys. Rev. A: At., Mol., Opt. Phys.* **1988**, 38, 3098–3100.

(66) Perdew, J. P. Density-functional approximation for the correlation-energy of the inhomogeneous electron-gas. *Phys. Rev. B: Condens. Matter Mater. Phys.* **1986**, 33, 8822–8824.

(67) Bader, R. F. W. *Atoms in Molecules: A Quantum Theory*; Oxford University Press: Oxford, U.K., 1994.

(68) Keith, T. A. AIMAll, ver. 17.11.14; TK Gristmill Software: Overland Park, KS, 2017.

(69) Contreras-García, J.; Johnson, E. R.; Keinan, S.; Chaudret, R.; Piquemal, J.-P.; Beratan, D. N.; Yang, W. NCIPLLOT: A program for plotting noncovalent interaction reagents. *J. Chem. Theory Comput.* **2011**, 7, 625–632.

(70) Humphrey, W.; Dalke, A.; Schulten, K. VMD: Visual molecular dynamics. *J. Mol. Graphics* **1996**, 14, 33–38.

(71) Mitoraj, M. P.; Parafiniuk, M.; Srebro, M.; Handzlik, M.; Buczek, A.; Michalak, A. Applications of the ETS-NOCV method in descriptions of chemical reactions. *J. Mol. Model.* **2011**, 17, 2337–2352.

(72) te Velde, G.; Bickelhaupt, F. M.; Baerends, E. J.; Fonseca Guerra, C.; van Gisbergen, S. J. A.; Snijders, J. G.; Ziegler, T. Chemistry with ADF. *J. Comput. Chem.* **2001**, 22, 931–967.

(73) *Chemcraft* version 1.7 (see <http://www.chemcraftprog.com>).